Magnetic and transport properties of nonequilibrium Eu-Fe thin films

1998 J. Phys.: Condens. Matter 10 5627

(http://iopscience.iop.org/0953-8984/10/25/013)

J. Phys.: Condens. Matter **10** (1998) 5627–5643. Printed in the UK PII: S0953-8984(98)89315-6

Magnetic and transport properties of nonequilibrium Eu–Fe thin films

T J Konno†, N Ogawa†§, K Wakoh†, K Sumiyama†, K Shoji†, H Onodera†, H Katoh‡ and K Suzuki†

† Institute for Materials Research, Tohoku University, Sendai 980-8577, Japan
‡ Department of Applied Physics, Faculty of Engineering, Tohoku University, Sendai 980-0945, Japan

Received 18 November 1997, in final form 9 March 1998

Abstract. We synthesized nonequilibrium Eu_xFe_{1-x} ($x = 0$–0.95) alloy thin films by co-evaporation and studied their structural, magnetic and transport properties using x-ray diffraction (XRD), Mössbauer spectroscopy, a SQUID and a DC four-probe method. The XRD and Mössbauer spectroscopy suggested that Fe atoms supersaturate in the bcc-Eu phase up to approximately 30 at.% Fe. On the other hand, these methods gave no indication of an extension in the solubility limit of Eu in the bcc-Fe phase. These nonequilibrium films possess the following properties: in the Fe-rich side, they exhibit a ferrimagnetic behaviour characterized by compensation temperatures at which magnetization is nonzero. In the Eu-rich side, the magnetization curve at 4.2 K exhibits a small, irreversible kink at about 8 T. At the same applied field, the magnetoresistance ratio (MR) changes irreversibly from positive to negative values, while subsequent runs yield only reversible, decreasing MR curves. These observations on Eu-rich films suggest that the dissolved Fe atoms disturb the long-range helical order of the Eu spins, and that the spin structure changes irreversibly at about 8 T. At present, it remains unclear whether the above magnetic and transport behaviours are caused by the magnetic moments of Fe or simply by a structural disorder.

1. Introduction

Nonequilibrium forms of rare-earth (RE)–transition-metal (TM) alloy systems exhibit a variety of magnetic and transport behaviours, as a number of studies reveal [1–3]. Systems consisting of heavy RE, such as Gd, Tb, Dy or Ho, and magnetic TM in particular have been the object of active research. Some studies have also dealt with nonequilibrium phases of Fe and light RE, including La [4], Pr [5] and Nd [6]. Thus, it is rather surprising to realize how little is actually known about the Eu–Fe system, despite the fact that Eu^{2+} is isoelectronic to Gd^{3+}. The lack of research in this area is partly due to the fact that the Eu–Fe phase diagram and the thermodynamic properties of the Eu–Fe system have not yet been experimentally determined [7, 8]. In fact, prior to a report regarding the formation of an $EuFe_2$ intermetallic phase [9], Eu and Fe were thought to be immiscible [10]. In addition, divalent Eu and Yb have always been regarded as exceptions from the systematic trend of trivalent RE elements, thereby drawing less attention.

Nevertheless, further study of the nonequilibrium Eu–Fe alloy system remains important. From a structural point of view, the possibility of amorphous phase formation needs to be

§ Present address: Daidoh Special Metals Co. Ltd, Tokai 477, Japan.

0953-8984/98/255627+17$19.50

examined, even though the driving force of that formation is not expected to be large [11]. Even if an amorphous phase is not realized, we can still anticipate an extension of the single-phase domains of the bcc-Eu and bcc-Fe phases, as observed in other immiscible systems [12, 13]. The magnetic and transport properties of these metastable phases have not been studied so far. In the Fe-rich side, we can expect the coupling between Eu and Fe to resemble that of Gd and Fe. If so, the Eu–Fe system should display ferrimagnetism, as the Gd–Fe system does [14]. Assuming that the dissolved Fe disturbs the helical order of the Eu moments [15, 16], then the magnetic and/or transport behaviours of the Eu–Fe alloy will differ from those of pure Eu.

Pure bulk Eu metal possesses a helical spin structure with a pitch of 3.5–3.6 a_0 (a_0: lattice parameter), and an interplanar turn angle of approximately 50° [15, 16]. The easy and hard magnetization directions of Eu are ⟨110⟩ and ⟨100⟩, respectively [17], and magnetization proceeds via lifting of the ordered moments, forming a conical spin structure [1, 18, 19]. The anisotropy energy of Eu is, however, small: previous experiments on single crystals indicate that the magnetization along ⟨110⟩ is only 5% to 10% greater than that along ⟨100⟩ [20, 21]. Neutron diffraction also shows that an applied field in a given direction effectively stabilizes the helical ordering in that direction [18]. Thus, the helical order of the bcc-Eu phase differs in nature from that of heavy lanthanides, i.e., Dy, Ho, and Er [22], because bcc-Eu lacks the combined presence of orbital moments and of an anisotropic crystal structure. Hence, a possible disorder brought in by the introduction of Fe will likely influence the magnetic structure of Eu metal in a straightforward way. We can also compare the magnetization behaviour of Eu–Fe polycrystalline thin films with that of single crystal films based upon available data given the fact that the anisotropy of the Eu metal is small. Accordingly, we made nonequilibrium Eu–Fe alloy films across the entire composition range by vapour synthesis and examined their physical properties. Our preliminary results indicated that the miscibilities in the Eu–Fe system are considerably extended in nonequilibrium alloys and that Eu-rich alloys have metamagnetic properties [23]. However, no systematic investigation of this system has been reported. The present article thus describes the structure and magnetic and transport properties of nonequilibrium Eu–Fe films in detail.

2. Experimental procedures

Eu–Fe nonequilibrium films of about 1 μm in thickness were prepared by co-evaporation. For the Fe source, we used zirconia and molybdenum for the inner and outer crucibles, respectively, and a molybdenum crucible for the Eu source. The crucibles were placed about 0.2 m away from the substrate position in a vacuum chamber. The base pressure of the chamber, obtained with a diffusion pump, was about 10^{-4} Pa. A few grams of Fe metal were heated by electron bombardment, while roughly the same amount of Eu metal was heated by conventional radiation from tungsten filaments. The purity of both metals was 99.99%. The deposition rates of Fe and Eu were assessed using an oscillation thickness monitor. We used polyimide films and Si(100) wafers as substrates for magnetic and structural characterization. The deposition was carried out at room temperature; however, we also prepared $Eu_{0.50}Fe_{0.50}$ alloys at 200, 300 and 400 °C in order to confirm that the films made at room temperature were indeed in a nonequilibrium state.

We employed a Rigaku x-ray diffractometer equipped with a Cu target, in the standard Bragg–Brentano geometry, for the x-ray diffraction (XRD) study. The specimens were tilted 8 degrees in order to avoid Si{400} reflection from the substrate. The chemical composition of the films was determined by electron probe microanalyser (EPMA). Mössbauer spectroscopy was carried out at room temperature with a constant

acceleration-type spectrometer using a ^{57}Co source doped in rhodium. The magnetic moments of the films up to 5 T were measured using a superconducting quantum interference device (SQUID) magnetometor, while those up to 23 T at 4.2 K were measured employing an extraction method in a hybrid-type high-field magnet [24]. In this report, we express the observed magnetic moments in terms of Bohr magnetons, μ_B, per atom, averaged over Eu and Fe according to composition. A standard DC four-probe method was used to measure the electrical resistivity of specimens at 4.2 K in magnetic fields up to 14 T applied in a parallel or perpendicular way to the current direction. The magnetoresistance ratio, MR, is defined by $\Delta\rho(H)/\rho(0) = [\rho(H) - \rho(0)]/\rho(0)$, where $\rho(H)$ is electrical resistivity as a function of magnetic field, H.

3. Results

3.1. Structure

Figure 1 shows a series of XRD patterns of the Eu_xFe_{1-x} films ($x = 0$ to 0.90). With increasing Eu content, the intensity of the Fe(110) peak decreases rapidly, and the peak almost disappears at $x = 0.28$. It should be noted that this value is close to the stoichiometric composition of the reported $EuFe_2$ phase. However, we did not observe any peak attributable to the intermetallic compound, nor did we detect a halo due to the presence of an amorphous phase. In contrast, the (110) and (200) peaks due to the bcc-Eu phase appear at $x = 0.19$ and 0.53, respectively. It should also be mentioned that the presence of peaks due to the EuO phase indicates that some of the Eu atoms are oxidized.

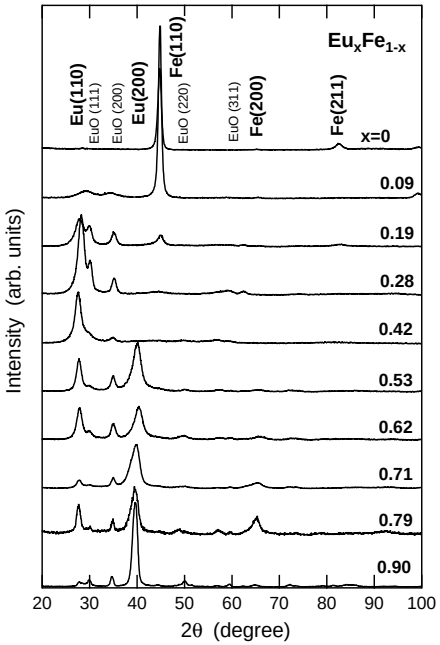

Figure 1. XRD patterns of Eu_xFe_{1-x} films. The samples were tilted 8° in order to avoid the (400) reflection from the Si substrates. Note that the Fe(110) peak almost vanishes at $x = 0.28$. The presence of peaks due to EuO indicates that a part of Eu was oxidized during sample handling.

Figure 2 shows the lattice parameters of the bcc-Fe phase estimated from the Fe(110) position and of the bcc-Eu phases estimated from the Eu(110) or Eu(200) peak position. The error bars are estimated from the full-width of the half-maximum of these peaks. The hatched area indicates a possible two-phase region, as suggested from the XRD and Mössbauer spectroscopic data. As shown here, the lattice parameter of the bcc-Fe phase (2.87 Å) does not change appreciably, while that of the bcc-Eu phase (4.58 Å) decreases slightly with increasing Fe content. The fact that the Fe lattice parameter does not change with Eu content suggests that the solubility of Eu in the bcc-Fe phase is negligibly small. On the other hand, the slight decrease of the Eu lattice parameter with increasing Fe content suggests that the Fe atoms do dissolve into the bcc-Eu phase. However, the decrease of the lattice parameter is substantially smaller than that expected from Vegard's law.

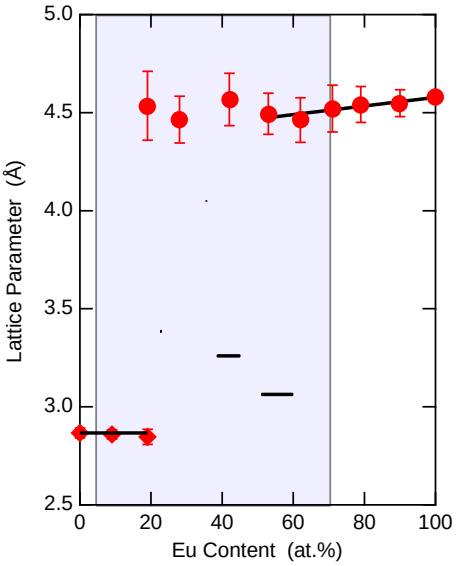

Figure 2. Lattice parameters of the bcc-Fe and bcc-Eu phases in the Eu_xFe_{1-x} films as functions of Eu content, estimated from Fe(110) and Eu(200) positions, respectively. The hatched area represents a possible two-phase region, as suggested by the XRD and Mössbauer spectroscopic data.

In order to confirm that Eu and Fe are alloyed by room temperature deposition, we deposited $Eu_{0.50}Fe_{0.50}$ films on heated substrates and compared the XRD intensities of the bcc-Fe phase. Figure 3 shows the XRD patterns of the films prepared at 25, 200, 300 and 400 °C. Since Eu metal is extremely vulnerable to oxidation, the formation of a EuO phase was inevitable. Nevertheless, the patterns reveal the effect of raises in substrate temperature, T_{sub}. Namely, the diffraction peaks due to the bcc-Fe phase become pronounced only when T_{sub} is as high as 400 °C, though a very weak Fe(110) peak is visible for the 300 °C-annealed sample. These observations indicate that a large amount of Fe atoms is alloyed with Eu upon co-evaporation at 25 °C and, to a lesser extent, at slightly higher temperatures.

To further examine the alloying behaviour, we carried out ^{57}Fe Mössbauer spectroscopy. Figure 4 shows the spectra obtained at room temperature for the Eu_xFe_{1-x} films with $x = 0.19$, 0.28, 0.42, 0.62 and 0.71. The absorption lines of Fe-rich samples are characterized by a sextet whose relative intensities are close to 3:4:1:1:4:3, as expected

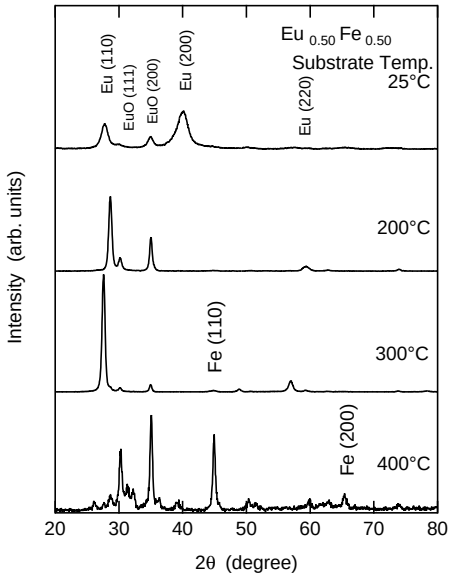

Figure 3. XRD patterns of the $Eu_{0.50}Fe_{0.50}$ films, deposited at 25, 200, 300 and 400 °C, showing that peaks due to the bcc-Fe phase, which appear at the substrate temperature of 300 °C, become pronounced at 400 °C.

from the in-plane magnetization of Fe. We fitted the observed spectra with four subspectra: (i) a sextet with an internal magnetic field, H_{int}, of 33 T, representing a contribution from the pure ferromagnetic Fe phase (hereafter designated as sextet 1), (ii) a sextet with an adjustable H_{int}, representing a signal from ferromagnetic Fe atoms, whose local molecular field is weaker than that of pure Fe (sextet 2), (iii) a doublet and (iv) a singlet. The doublet and singlet represent contributions from nonmagnetic Fe dissolved in the bcc-Eu phase. The presence of these two subspectra due to the nonmagnetic Fe is evident in the obtained spectra of Eu-rich samples, while its presence is not clear in the case of Fe-rich samples. Nevertheless, we used all of the above-mentioned four subspectra for the fitting. Accordingly, there are large errors in the Mössbauer parameters of a minor component(s), even though the fitting routine itself converged well for all the spectra. These errors are indicated in table 1. We also assumed that the full-width at half-maximum (FWHM) is the same for the four subspectra for a given composition. Thus, the obtained FWHM values represent the value of a major component(s) in a given spectrum.

Figure 5 shows the relative intensities of the four standard subspectra as functions of the Eu content of the films, while table 1 shows Mössbauer parameters employed for the fitting. As the figure shows, the intensity of sextet 1 monotonically decreases with the increase in Eu content, while that of sextet 2 reveals a broad peak in the composition range of 40–60%. Above Eu $\approx$ 70%, however, the sextets disappear. Concurrently, the relative intensities of the singlet and doublet gradually increase. These changes in intensity indicate that portions of Eu and Fe are indeed alloyed. It should be mentioned that in the Eu concentration range of 40–60%, the sextets do possess nonzero intensities, but that the corresponding XRD patterns of these films do not indicate peaks due to the bcc-Fe phase. This observation implies that the Fe atoms in these middle compositions exist in small bcc-Fe particles. Therefore, it is possible to assume that, in the films richer in Eu, smaller Fe particles exist in a superparamagnetic state and exhibit a ferromagnetic behaviour at low temperatures,

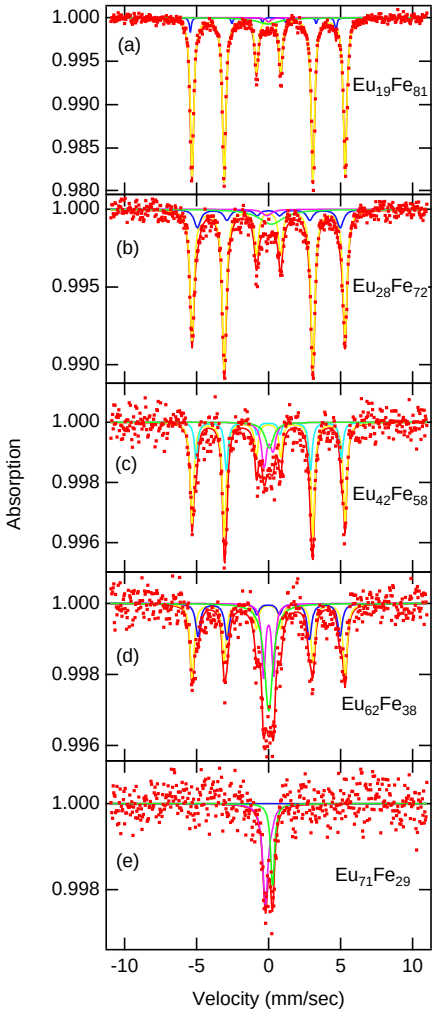

Figure 4. ^{57}Fe Mössbauer spectra of the Eu_xFe_{1-x} films at room temperature. Each spectrum was fitted using two sextets, a doublet and a singlet (see text). The poor signal-to-noise ratios of these Eu-rich films spectra are due to the strong absorption by Eu. Note that the sextet disappears at $x = 71\%$.

especially in the samples with Eu $\geqslant$ 70%. Unfortunately, the very strong absorption of γ-rays by Eu made it very difficult to obtain meaningful results for the Eu-rich samples. Nevertheless, a comparison of the magnetic and transport behaviours of the annealed and unannealed Eu-rich films did suggest that Eu and Fe in these compositions are alloyed, as shown later (figures 7 and 11).

The Mössbauer parameters listed in table 1 deserve some comments. The hyperfine field, H_{hf}, of sextet 2 is 30–31 T. In Fe-based amorphous alloys, H_{hf} is known to correlate with heat of formation, ΔH. Namely, it is close to 30 T for a system with positive ΔH, while it decreases for a system with negative ΔH. For example, in the La–Fe system where ΔH is positive, the observed H_{hf} is 29.8 T, while in the Lu–Fe system, in which ΔH is negative, the H_{hf} is 19.5 T [25]. Thus, the observed large H_{hf} for the Eu–Fe thin films is

Table 1. Room temperature Mössbauer parameters obtained by the spectral analysis of the profiles of the co-evaporated Eu_xFe_{1-x} films shown in figure 4. H_{hf} is the hyperfine field, IS is the isomer shift, QS is the quadruple splitting and FWHM is the full-width at half-maximum. The IS, QS and FWHM are given relative to bcc-Fe. The values in parentheses are for subspectra whose fraction of the total absorption is less than 2%. The estimated errors depend on the relative intensity of a subspectrum, except that the error in FWHM is ± 0.05 mm s^{-1} for all the compositions (see text).

		19 at.% Eu	28 at.% Eu	42 at.% Eu	62 at.% Eu	71 at.% Eu
Sextet 2	H_{hf} (T)	(29 ± 1)	30.1 ± 0.2	31.3 ± 0.2	31.3 ± 0.2	(30 ± 1)
	IS (mm s^{-1})	(0.1 ± 0.1)	-0.1 ± 0.1	0.03 ± 0.05	-0.03 ± 0.05	(0 ± 0.1)
	QS (mm s^{-1})	(-0.1 ± 0.3)	0.0 ± 0.1	0.03 ± 0.05	0.02 ± 0.05	(0 ± 0.1)
Doublet	IS (mm s^{-1})	(0.0 ± 0.1)	(-0.2 ± 0.1)	0.00 ± 0.05	0.00 ± 0.02	0.01 ± 0.02
	QS (mm s^{-1})	(0.6 ± 0.3)	(1.1 ± 0.3)	0.7 ± 0.1	0.67 ± 0.05	0.58 ± 0.5
Singlet	IS (mm s^{-1})	(0.0 ± 0.1)	(-0.1 ± 0.1)	-0.10 ± 0.05	-0.03 ± 0.02	-0.01 ± 0.02
All subspectra	FWHM (mm s^{-1})	0.29	0.35	0.33	0.38	0.36

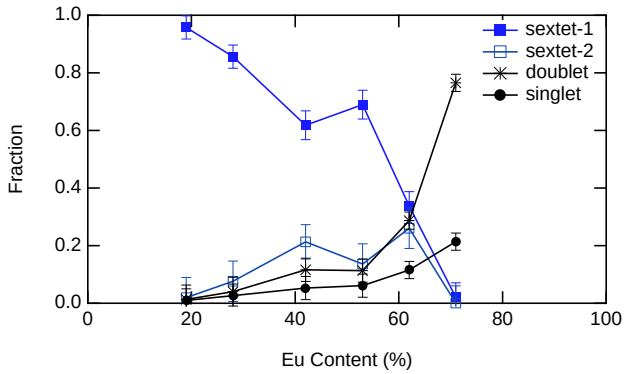

Figure 5. Relative intensities of the standard subspectra, used to fit the ^{57}Fe Mössbauer spectra of the Eu_xFe_{1-x} films. Estimated errors are also shown. The sextets are significant up to about 60% Eu, while the paramagnetic components increase as Eu content increases.

in qualitative agreement with the positive ΔH of the system. In addition, the quadrupole splitting, QS, of sextet 2 is very small, indicating that a departure from cubic symmetry around Fe atoms in the bcc-Fe phase is small. On the other hand, the QS of the doublet is 0.6–0.7 mm s^{-1}, indicating that nonmagnetic Fe atoms are surrounded by an anisotropic environment. Finally, the isomer shift (IS) of the doublet and singlet is mostly negative. This is in qualitative agreement with the values predicted by Miedema and van der Woude [26]. Namely, the IS of Fe is negative when Fe atoms are surrounded by Y, which is chemically similar to Eu [27].

3.2. Magnetic properties

Figure 6(a) shows magnetic moments, M, per atom for the Eu_xFe_{1-x} films with $x = 0.09$–0.42 at $H = 1$ T as functions of temperature, T. The moment of $Eu_{0.09}Fe_{0.91}$ increases with increasing temperature, while that of $Eu_{0.19}Fe_{0.81}$ exhibits a minimum at about 70 K, followed by a gradual increase. For $Eu_{0.28}Fe_{0.72}$, there is still a shallow minimum around 170 K, even though the overall curve is dominated by a monotonic decrease. The

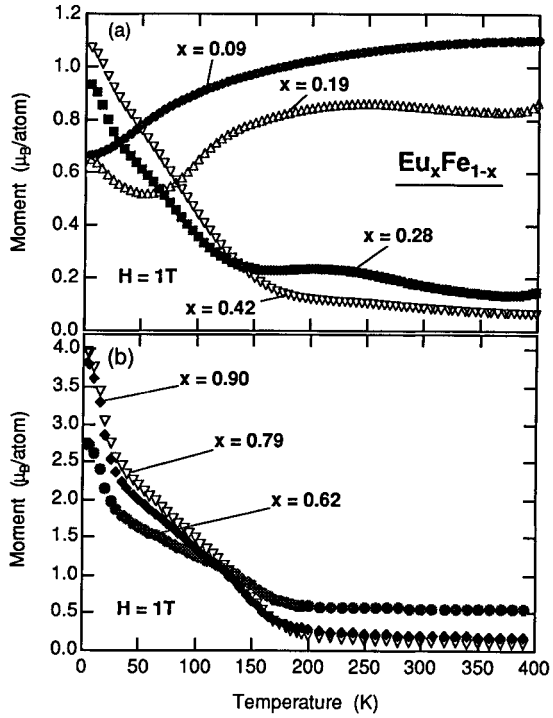

Figure 6. Magnetic moments as functions of temperature at $H = 1$ T. (a) Fe-rich films exhibit compensation temperatures at which the moments are nonzero, while (b) Eu-rich films show only a monotonic decrease with temperature.

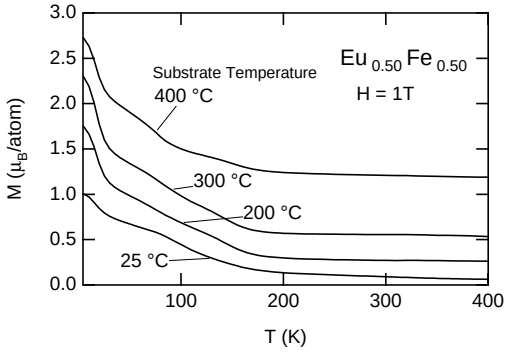

Figure 7. Magnetic moments as a function of temperature for the $Eu_{0.50}Fe_{0.50}$ films deposited at 25, 200, 300 and 400 °C, indicating that the constant component due to the bcc-Fe phase increases as the substrate temperature increases.

M–T curves for films with more than 40% Eu exhibit a monotonic decrease up to about 200 K, followed by a nearly constant value. Figure 6(b) shows the *M–T* curves of the Eu-rich side of the Eu_xFe_{1-x} films ($x = 0.62$–0.90). The moments decrease rapidly with increasing temperature up to about 30 K, then gradually decrease and become almost constant above 180 K. These features are in qualitative agreement with the behaviour reported for pure Eu [25], except that (i) the absolute magnetic moment at 4.2 K is smaller

than 7 μ_B (the value expected from pure Eu), and (ii) the peak at 95 K arising from the helical ordering of the moments in the pure bcc-Eu phase [1, 17, 28] is not present. As for the Eu-rich films, the observed shape of their M–T curves is also similar to that found in the Eu-rich EuO films made by vapour-phase synthesis. That is, the Curie temperature of the Eu-rich EuO film is approximately 150 K and the M–T curve shows a shoulder at about 100 K [29].

Figure 7 shows the M–T curves at $H = 1$ T for the $Eu_{0.50}Fe_{0.50}$ films deposited at 25, 200, 300 and 400 °C. The effect of raising T_{sub} is to add a constant magnetic moment to a monotonically decreasing curve. Considering that the Néel point of the bcc Eu phase is about 90 K [18, 30], we can assume that the decreasing component in the low temperature region, 5–150 K, arises from the bcc-Eu phase and also possibly from the minor EuO phase, while we may also presume that the constant component is due to the bcc-Fe phase. The constant part of the 400 °C-deposited sample is about 1.2 ± 0.1 μ_B, a value that is reasonably close to the expected value of 1.1 μ_B if all the Fe atoms are segregated to form the bcc-Fe phase. The decrease of this constant component with decreasing T_{sub} indicates that Fe is progressively dissolved into the Eu phase during deposition as the substrate temperature is lowered, and that the dissolved Fe atoms do not appreciably contribute to the magnetization of the sample.

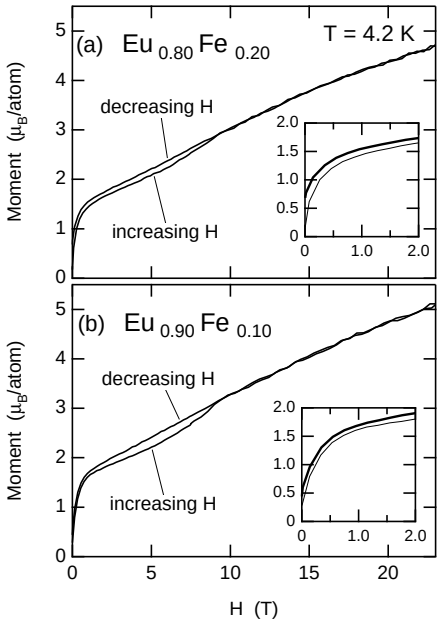

Figure 8. Magnetic moments as a function of external field at 4.2 K for (a) $Eu_{0.80}Fe_{0.20}$ and (b) $Eu_{0.90}Fe_{0.10}$ films, showing a hysteric behaviour. The insets show the curves in the low field regions, indicative of residual magnetic moments at zero field.

Figures 8(a) and (b) show the magnetic moments per atom at 4.2 K as functions of H for $Eu_{0.80}Fe_{0.20}$ and $Eu_{0.90}Fe_{0.10}$ films, respectively. The curves show that, with increasing H, the moment initially rises to about 1.5 μ_B, then gradually increases and exhibits a small, but distinct, 'kink' at around $H = 8$ T. After that, the moment increases monotonically and does not saturate even at $H = 23$ T. With decreasing magnetic field, the moment decreases

monotonically, without exhibiting any kink. Thus, the kink at about 8 T appears irreversibly in the magnetization curve. Furthermore, the insets show that both samples exhibit residual moments of about 0.5 μ_B/atom. No kink is observed in the magnetization curve of pure Eu [20, 21], and the presence of a kink in the magnetization curve of the Eu–Fe film suggests that the introduction of Fe alters the magnetic behaviours of pure Eu.

3.3. Transport properties

Figure 9 shows the longitudinal (L-) and transverse (T-) MR of the $Eu_{0.95}Fe_{0.05}$ film at 4.2 K. We measured MR in both increasing field, up to 14 T, and decreasing field, and repeated the measurements twice to monitor any possible hysteric behaviour. From the figure, we can see that in the first run, L-MR increases to about 5% at 8 T, and then decreases rapidly, giving about −1% at 14 T. In the decreasing field, L-MR deviates from that in the increasing field at about 8 T, resulting in a residual value of about 4–5%. In the second run, L-MR exhibits an almost identical behaviour to that observed in the latter half (decreasing field) of the first run. Likewise here, T-MR exhibits a small maximum at about 5 T, followed by a large decrease. In the decreasing field, T-MR also deviates considerably from the initial curve, giving a residual value of about −2%.

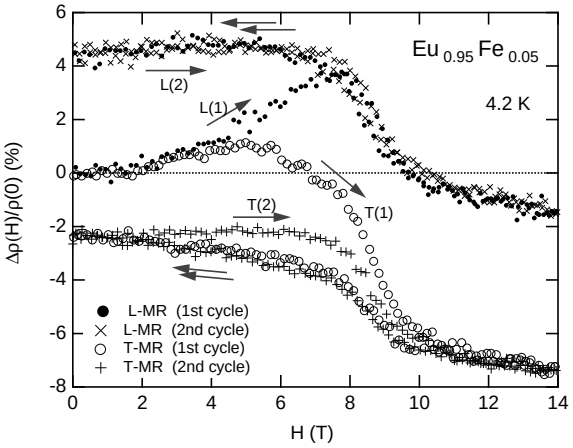

Figure 9. L- and T-MR of the $Eu_{0.95}Fe_{0.05}$ film at 4.2 K. L(1), L(2), T(1) and T(2) indicate L-MR (first cycle), L-MR (second cycle), T-MR (first cycle) and T-MR (second cycle), respectively. Note that the MR curves comprise irreversible and reversible components.

Figure 10 shows L-MR at 4.2 K of Eu_xFe_{1-x} films with $x = 0.90, 0.85, 0.70, 0.60$. As shown, the L-MR curves of all specimens exhibit a positive-to-negative transition at about 8 T, as well as residual MR.

Figure 11 shows L-MR at 4.2 K of $Eu_{0.50}Fe_{0.50}$ films deposited at 25, 200, 300 and 400 °C. The L-MR of the 25 °C-deposited sample exhibits a positive-to-negative transition at $H = 8$ T, a behaviour that constitutes the essential feature found in other Eu–Fe films. The 200 °C-deposited specimen, on the other hand, departs from this behaviour and exhibits only positive values. Finally, the L-MR of the 400 °C deposited specimen shows only a monotonic increase with increasing field. This observation is in good agreement with the reported findings on the L-MR of pure Eu measured up to $H = 8$ T, which also exhibits a monotonic increase [31]. This leads us to conclude that the positive-to-negative transition

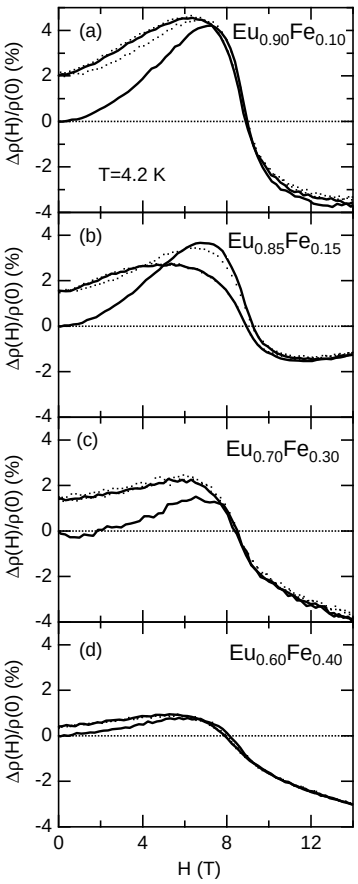

Figure 10. L-MR of the Eu_xFe_{1-x} films at 4.2 K. The solid and dotted curves correspond to the first and second cycle, respectively. All specimens exhibit an anomalous positive-to-negative change at about 8 T.

in MR at $H = 8$ T, as well as the kink in the magnetization curve, are intrinsic properties of the nonequilibrium Eu–Fe films.

4. Discussion

4.1. Structure

The structural characterization of the vapour-synthesized Eu–Fe films reveals the following results: (i) the solubility of Eu in the bcc-Fe phase is not extended to an appreciable degree, (ii) the formation of $EuFe_2$ or of an amorphous phase does not take place and (iii) in Eu-rich films (Eu $\geqslant$ 70%), a majority of Fe atoms dissolve into the bcc-Eu phase. In addition, all the films contain an EuO phase as a minor component.

The fact that we did not observe an amorphous phase corresponding to $EuFe_2$ reveals a contrast with the behaviour of the Gd–Fe system [32, 33]. However, this may be justified

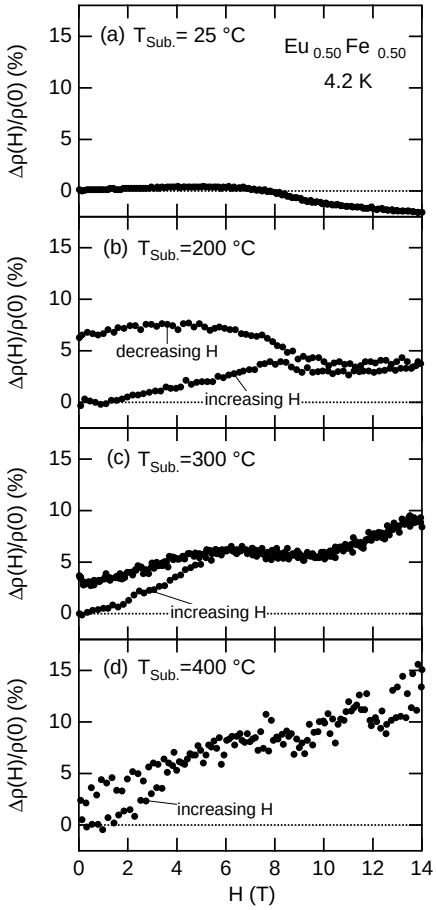

Figure 11. L-MR of the $Eu_{0.50}Fe_{0.50}$ films deposited at 25, 200, 300, and 400 °C, indicating that the anomalous effect disappears as the substrate temperature increases.

by the small driving force in this system [11]. In fact, a system with a large glass-forming ability is generally associated with a large enthalpy change upon mixing [34] and normally exhibits a deep eutectic phase diagram [35]. The comparison of the Eu–Fe phase diagram with other RE–Fe phase diagrams [8] shows that the Eu–Fe system does not fall into such a class. We may thus conclude that vapour quenching does not produce a chemical bonding comparable to that which exists in $EuFe_2$ or in the Gd–Fe system due to a lack of thermodynamical driving force.

4.2. Magnetic properties of Fe-rich films

The M–T curves at $H = 1$ T for Fe-rich samples (up to 30% Eu) are characterized by the presence of a shallow minimum, which suggests that Eu and Fe moments align in an anti-parallel direction at different magnetic transition temperatures. This is a ferrimagnetic behaviour found in a number of amorphous RE–TM systems, including Gd–Fe, where

the M–T curves exhibit a clear compensation temperature, T_{comp} [3, 36, 37]. The antiparallel arrangement of the magnetic moments of Fe and divalent Eu is expected from the indirect coupling scheme proposed by Campbell [38]. However, in the present study, the magnetization is nonzero at T_{comp}. It has not yet been possible to determine with certainty the origin of the nonzero moment, but we suspect that these moments arise from either (i) the non-collinear distribution (within a cone) of the Fe spins, or (ii) the heterogeneous structure of the films, which are composed of ferromagnetic bcc-Fe and EuO phases and a ferrimagnetic Eu–Fe alloy, or (iii) a combination of both (i) and (ii). The first mechanism is thought to be the origin of the nonzero moments at T_{comp} of a Dy–Fe amorphous alloy [39, 40]. It is known that Fe–Fe exchange coupling is a sensitive function of interatomic separation, giving rise to the conical distribution of Fe moments, while the parallel alignment of Co spins is said to be due to the positive distribution of Co–Co exchange fields [39–41]. On the other hand, the second mechanism can be responsible for the appearance of the compensation temperature. For instance, calculations of antiferromagnetically coupled multilayers, such as Gd and Fe, indicate that the coupled phases can exhibit a ferrimagnetic behaviour [42]. Thus, we can expect that divalent Eu, which is isoelectronic to Gd, and Fe to behave similarly. Furthermore, when such ferrimagnetic behaviour is superimposed on the ferromagnetic behaviour of Fe, nonzero compensation temperatures can also be expected.

4.3. Magnetic properties of Eu-rich films

We will start by discussing the initial rise in the magnetization curve and overall susceptibility of Eu-rich films. The magnetization curve of a single crystal Eu in the [100] direction shows an initial rise to about 0.6 μ_B/atom at 0.8 T due to the formation of a single domain [21]. Neutron diffraction indicates that a small magnetic field of below 1 T is sufficient to create a single domain state [18]. Thus, it is reasonable to ascribe the initial rise of about 1.5 μ_B/atom shown in the M–H curve (figure 8) to single domain formation, though this rise is slightly greater than the value reported for pure Eu. This difference might stem from the ferromagnetic EuO phase that acts as a minority component. Once the single domain state is established, the overall susceptibility of the Eu-rich Eu–Fe alloy becomes similar to that of the pure Eu. Namely, the value of the moments of pure Eu in the [110] direction is approximately 3.8 μ_B/atom at 23 T [21], a value comparable to that observed for the $Eu_{0.90}Fe_{0.10}$ film of about 5 μ_B/atom at 23 T (figure 8).

A kink in the magnetization curve of RE–TM alloys is often associated with a change in noncollinear spin structure, such as spin flopping [43, 44]. The noncollinear spin structure in amorphous RE–TM alloys can be categorized into two classes, the first in which both RE and TM possess magnetic moments, and the second in which only RE possesses the moments. Noncollinearity in the former arises from antiferromagnetic coupling between RE and TM moments and from random anisotropy [39, 41], while in the latter it arises solely from random anisotropy fields [45, 46]. In the present work, we were not able to determine, by Mössbauer spectroscopy, whether or not the introduced Fe atoms possess magnetic moments in the Eu-rich alloys because of the strong absorption of γ-rays by the Eu atoms. If the Fe atoms do possess moments, then the antiferromagnetic Eu–Fe coupling must compete with similarly antiferromagnetic Eu-Eu coupling. The former is a short-range effect [38], while the latter constitutes a long-range interaction via conduction electrons. Thus, the randomly distributed Fe moments are likely to disturb the helical order and produce a frustrated spin structure. On the other hand, if the Fe atoms do not possess magnetic moments, then the helical order is disturbed by the structural disorder alone.

4.4. Transport properties of Eu-rich films

The observed MR behaviours of Eu-rich films are in striking contrast to the positive and monotonically increasing MR of pure Eu. In this section, we will briefly review several important mechanisms and propose a model that could eventually explain anomalous behaviours.

Jánôs *et al* showed that the L-MR of pure Eu up to 8 T increases monotonically and exhibits a hysteresis in the 0–2 T range [31]. Boyarskii and Dikovskii separated the irreversible components of L- and T-MR of pure Eu [47], and ascribed the irreversibility observed up to 2 T to (i) the formation of a single domain state, and (ii) the possible irreversible reorientation of the helix axis. A positive MR at a small applied field due to the formation of a single domain has also been reported to exist in other RE including Nd [48] and Gd [49]. We thus know that the irreversible MR components of pure Eu are significant up to about 0.8–2 T. However, the irreversible MR components of Eu–Fe alloys manifest themselves up to about 8 T, so it is difficult to ascribe them to the formation of a single domain. Our magnetization measurements also indicate that a single domain state is probably established within the initial 1 T. Furthermore, the presence of a minority EuO phase should not have any effect above 1 T since EuO is ferromagnetic and its moments saturate easily.

A positive MR can arise also from normal MR (a change of resistivity by the Lorentz force acting on the conduction electron trajectories) [49]. This mechanism is found to be operative in REs with a helical spin structure, including Tb and Ho [50, 51]. Single crystal Gd also exhibits positive MR at 4.2 K due to normal MR [49, 52]. However, even though the MR of pure Eu is likely to be caused by normal MR, this mechanism does not appropriately explain the irreversible positive-to-negative MR change of the Eu–Fe alloy. Also, the collision frequency of conduction electrons in a disordered alloy is much higher than the cyclotron frequency. Thus it is quite unlikely that normal MR plays a significant role in the MR behaviour of Eu–Fe alloys.

Besides normal MR, there are two effects that can influence the MR of REs with a helical spin structure: the superzone effect and the spin fluctuation effect. The former arises from the disappearance of the superzone [53–56] due to a transition from helical to fan structures, as observed in Ho [57, 58]. However, the magnetization measurements of the Eu–Fe alloys do not indicate a helical to fan transition, and the mechanism based on superzone formation must therefore be discarded.

Hence, we were led to propose that the spin fluctuation effect is the dominant factor influencing the transport behaviour of Eu–Fe alloys. Calculations by Yamada and Takada, based on the spin wave scattering model, indicate that the MR of a simple two-sublattice antiferromagnet increases with field ($\propto H^2$), since spin fluctuation in the sublattice antiparallel to the field direction increases with the applied field [59, 60]. This effect prevails until the spin-flop transition occurs, after which the MR decreases. On the basis of this model we put forth the assumption that a small number of spins are initially in an unstable state, thereby contributing to a positive MR. With increasing field, the spins eventually flop to form a stable conical spin structure, resulting in a negative MR.

Figure 12 shows a tentative schematic model of the spin structure of Eu-rich Eu–Fe alloys. As mentioned before, the moments in pure Eu align helically at an interplanar turn angle of approximately 50° [15, 16, 18] In Eu–Fe alloys, the randomly dissolved Fe atoms scatter the Eu moments out of the helical plane, creating a metastable spin configuration, as indicated in figure 12(a). The application of a magnetic field lifts most of the Eu moments in the field direction, but some of the Eu moments cannot tilt in that direction due to

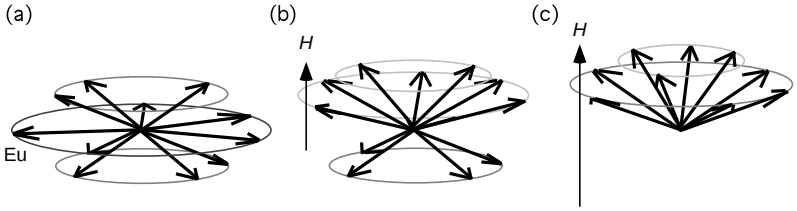

Figure 12. Schematic model of the tentatively proposed spin structure of the Eu–Fe alloy. (a) Eu spins are displaced from the helical plane because of Fe impurities; (b) with an external magnetic field, most of the Eu spins tilt in the field direction, while some remain unchanged. Spins in the anti-parallel direction give rise to a positive MR; (c) above the critical field, the anti-parallel spins flop, forming a conical spin structure.

the presence of impurities (figure 12(b)). Above the critical field, the minority spins flop, forming a conical ferromagnetic configuration which gives rise to an overall negative MR (figure 12(c)). The presence of these minority spins and their flopping are also the origin of the kink in the magnetization curve.

In the present work, we were not able to determine whether or not the introduced Fe atoms possess magnetic moments in the Eu-rich films. Thus, the role of Fe impurities in the above postulate could best be clarified by similar magnetization and MR experiments on an Eu–TM system with nonmagnetic TM. This study has already been undertaken and will be the subject of a forthcoming paper.

5. Conclusion

We synthesized nonequilibrium Eu_xFe_{1-x} ($x = 0$-0.95) alloy thin films by co-evaporation. In general, these films are composed of the bcc-Fe, bcc-Eu and minor EuO phases. The XRD and Mössbauer spectroscopy indicate that Fe atoms dissolve rather extensively in the bcc-Eu phase ($x > 0.7$), but reveal no appreciable extension of the solubility limit of Eu in the bcc-Fe phase. In the Fe-rich side ($x \leqslant 0.3$), the Fe and Eu moments couple antiferromagnetically, and the films exhibit a ferrimagnetic character, with the M–T curves showing nonzero magnetic moments at compensation temperatures. In the Eu-rich side, the magnetization curves show a kink at about 8 T and the MR changes from positive to negative values. These anomalous features are in marked contrast with the behaviour of pure Eu, suggesting that the Fe atoms disturb the long-range helical order of Eu spins. At present, it remains unclear whether or not these features are caused by the direct interaction of Fe moments with the helically ordered Eu moments or merely by the presence of Fe atoms which change the interaction among the Eu moments and thereby indirectly disturb the helical order of Eu.

Acknowledgments

The authors wish to thank Mr Y Murakami for the EPMA analysis, performed in Laboratory for Developmental Research of Advanced Materials, IMR, Tohoku University. High field magnetization measurements were performed in High Field Laboratory for Superconducting Materials, Tohoku University. This work was supported by the grants-in-aid for scientific research (A-2: 08405043 and C:08875127) and for scientific research on priority areas (06244102), provided by the Ministry of Education, Science, Sports and Culture of Japan.

References

[1] McEwen K A 1978 *Handbook on the Physics and Chemistry of Rare Earths* vol 1, ed K A Gschneidner Jr and L Eyring (Amsterdam: North-Holland) p 411
[2] Rhyne J J 1979 *Handbook on the Physics and Chemistry of Rare Earths* vol 2, ed K A Gschneidner Jr and L Eyring (Amsterdam: North-Holland) p 259
[3] Buschow K H J 1984 *Handbook on the Physics and Chemistry of Rare Earths* vol 7, ed K A Gschneidner Jr and L Eyring (Amsterdam: North-Holland) p 265
[4] Wakabayashi H, Goto T, Fukamichi K and Komatsu H 1990 *J. Phys.: Condens. Matter* **2** 417
[5] Croat J J 1981 *J. Appl. Phys.* **52** 2509
[6] Taylor R C, McGuire T R, Coey J M D and Gangulee A 1978 *J. Appl. Phys.* **49** 2885
[7] Kubaschewski O 1982 *Iron Binary Phase Diagrams* (Berlin: Springer) p 38
[8] Okamoto H 1993 *Phase Diagrams of Binary Iron Alloys* ed H Okamoto (Materials Park, OH: ASM) p 341
[9] Ning Y-T, Zhou X-M, Zhen Y, Chen N-Y, Xu H and Zhu J-Z 1989 *J. Less-Common Met.* **147** 167
[10] Moffatt W G 1976 *Handbook of Binary Phase Diagrams* vol 3 (Schenectady, NY: Genium)
[11] Miedema A R 1976 *J. Less-Common Met.* **46** 167
[12] Sumiyama K 1991 *Phys. Status Solidi* a **126** 291
[13] Konno T J and Sinclair R 1993 *Mater. Chem. Phys.* **35** 99
[14] Orehotsky J and Schröder K 1972 *J. Appl. Phys.* **43** 2413
[15] Olsen C E, Nereson N G and Arnold G P 1962 *J. Appl. Phys.* **33** 1135
[16] Nereson N G, Olsen C E and Arnold G P 1964 *Phys. Rev.* **135** 176
[17] Mackintosh A R 1971 *J. Physique Coll.* **32** C1 487
[18] Millhouse A H and McEwen K A 1973 *Solid State Commun.* **13** 339
[19] Nagamiya T, Nagata K and Kitano Y 1962 *Prog. Theor. Phys.* **27** 1253
[20] Johansson T, McEwen K A and Touborg P 1971 *J. Physique Coll.* **32** C1 372
[21] McEwen K A, Cock G J, Roeland L W and Mackintosh A R 1973 *Phys. Rev. Lett.* **30** 287
[22] Koehler W C 1965 *J. Appl. Phys.* **36** 1078
[23] Ogawa N, Sumiyama K, Konno T J, Katoh H, Wakoh K and Suzuki K 1997 *Physica* B **237/238** 289
[24] Nakagawa Y, Noto K, Hoshi A, Miura S, Watanabe K and Muto Y 1984 *J. Physique Coll.* **45** C1
[25] van der Kraan A M and Buschow K H J 1982 *Phys. Rev.* B **25** 3311
[26] Miedema A R and van der Woude F 1980 *Physica* B **100** 145
[27] van der Kraan A M and Buschow K H J 1983 *Phys. Rev.* B **27** 2693
[28] Bozorth R M and Van Vleck J M 1960 *Phys. Rev.* **118** 1493
[29] Konno T J, Ogawa N, Wakoh K, Sumiyama K and Suzuki K 1996 *Japan. J. Appl. Phys.* **35** 6052
[30] Cohen R L, Hüfner S and West K W 1969 *Phys. Rev.* **184** 263
[31] Jánôs S, Feher A and Flachbart K 1977 *Phys. Status Solidi* b **81** K19
[32] Rhyne J J, Schelleng J H and Koon N C 1974 *Phys. Rev.* B **10** 4672
[33] Vittoria C, Lubitz P and Ritz V 1978 *J. Appl. Phys.* **49** 4908
[34] Elliott S R 1984 *Physics of Amorphous Materials* 2nd edn (Harlow: Longman) p 38
[35] Allen J W, Wright A C and Connell G A N 1980 *J. Non-Cryst. Solids* **42** 509
[36] Kirchmayr H R and Poldy C A 1979 *Handbook on the Physics and Chemistry of Rare Earths* vol 2, ed K A Gschneidner Jr and L Eyring (Amsterdam: North-Holland) p 55
[37] Hansen P, Klahn S, Clausen C, Much G and Witter K 1991 *J. Appl. Phys.* **69** 3194
[38] Campbell I A 1972 *J. Phys. F: Met. Phys.* **2** L47
[39] Arrese-Boggiano R, Chappert J, Coey J M D, Liénard A and Rebouillat J P 1976 *J. Physique Coll.* **37** C6 771
[40] Rebouillat J P, Lienard A, Coey J M D, Arrese-Boggiano R and Chappert J 1977 *Physica* **86–88B** 773
[41] Coey J M D, Chappert J, Rebouillat J P and Wang T S 1976 *Phys. Rev. Lett.* **36** 1061
[42] Camley R E 1989 *Phys. Rev.* B **39** 12 316
[43] Hiroyoshi H, Kato H, Yamada M, Saito N and Nakagawa Y 1987 *Solid State Commun.* **62** 475
[44] Yamada M, Kato H, Yamamoto H and Nakagawa Y 1988 *Phys. Rev.* B **38** 620
[45] Heiman H and Kazama N 1978 *J. Appl. Phys.* **49** 1686
[46] Coey J M D, McGuire T R and Tissier B 1981 *Phys. Rev.* B **24** 1261
[47] Boyarskii L A and Dikovskii V Y 1976 *Sov. J. Low Temp Phys.* **2** 632
[48] Nagasawa H 1972 *Phys. Lett.* **41A** 39
[49] McEwen K A, Webber G D and Roeland L W 1977 *Physica* **86–88B** 531
[50] Singh R L, Jericho M H and Geldart D J W 1976 *Phys. Rev.* B **13** 4949
[51] Singh R L 1977 *Phys. Rev.* B **15** 4174

[52] Maezawa K, Mizushima T, Mori K, Sato K, Saito Y and Wakabayashi S 1979 *J. Phys. Soc. Japan* **47** 585
[53] Miwa H 1962 *Prog. Theor. Phys.* **28** 208
[54] Mackintosh A R 1962 *Phys. Rev. Lett.* **9** 90
[55] Miwa H 1963 *Prog. Theor. Phys.* **29** 477
[56] Elliott R J and Wedgwood F A 1963 *Proc. Phys. Soc.* **81** 846
[57] Mackintosh A R 1964 *Solid State Commun.* **2** 383
[58] Akhavan M and Blackstead H A 1976 *Phys. Rev.* B **13** 1209
[59] Yamada H and Takada S 1973 *J. Phys. Soc. Japan* **34** 51
[60] Yamada H and Takada S 1973 *Prog. Theor. Phys.* **49** 1401